IOSR Journal of Applied Chemistry (IOSR-JAC)
e-ISSN: 2278-5736.Volume 14, Issue 1 Ser. I (January. 2021), PP 11-25
www.iosrjournals.org

Correlations between the basicity and the fractal dimension of Rh-nanoparticles supported on Al_2O_3, TiO_2 and WO_3

Gianina Dobrescu, Florica Papa, Irina Atkinson, Daniela Culita, Ioan Balint
(Romanian Academy, Institute of Physical Chemistry "Ilie Murgulescu", Spl. Independentei 202, PO Box 12-194, RO-060021, Bucharest, Romania)

Abstract:
Background*: Catalysts are successful candidates to be described by fractal theory, as they are usually materials with higher BET area, very irregular, with a shape difficult to describe as a convolution of planar surfaces. Enhancing catalytic activity for DRM of catalysts implies obtaining catalysts with higher basicity. The relation between the catalysts basicity and the fractal dimension will be investigated.*
Materials and Methods*: Highly dispersed Rh nanoparticles on various supports like Al_2O_3, TiO_2 and WO_3, metal loading 1% was obtained by impregnation of the support powder with water dispersed rhodium nanoparticles synthesized by modified alkaline polyol method. The morphology, size, structure, texture, the basic sites surface distribution of the catalysts and rhodium-support interactions were characterized by transmission electron microscopy, by X-ray diffraction (XRD), nitrogen adsorption-desorption isotherm analysis, CO-chemisorption, thermo-programmed desorption (TPD) of CO2 and by fractal analysis.*
Results*: Fractal dimensions of the Al_2O_3, TiO_2, WO_3, Rh/Al_2O_3, Rh/TiO_2 and Rh/WO_3 catalysts were computed using TEM images analysis; nitrogen adsorption isotherms analysis was used to compute the fractal dimension of the catalysts before and after CO_2-TPD. The idea of this paper is to correlate the fractal dimension of the support/catalyst with chemical or morphological properties of them, such as basicity or specific surface to offer some insights in studying the metal-support interaction. Results show that adding Rh-nanoparticles on supports will decrease the system fractal dimension as a prove of Rh encapsulation via SMSI. Also, meanwhile the number of weak and medium basic sites decrease as the fractal dimension increases, the number of strong and of the total basic sites increase as the surface fractal dimension increases. This behavior is related to Rh encapsulation at high fractal dimensions or to the blockage of the surface pores and irregularities by surface restructuring at low fractal dimensions.*
Conclusion: *A direct relation between the support and Rh/support fractal dimension and the basicity of the catalysts, obtained via CO_2-TPD was emphasized. A method to enhance catalysts' basicity is to use supports with higher fractal dimension; the paper proved that even if, by adding nanoparticles, such as Rh, the catalyst fractal dimension will be lowered by encapsulation, it is the same encapsulation, consequence of strong metal-support interaction (SMSI), that will favor strong basicity sites formation when the oxide fractal dimension is high enough.*
Key Word*: Nanoparticles; Fractal; Basicity; CO_2-TPD; TEM; Adsorption Isotherms.*

Date of Submission: 06-01-2021 Date of Acceptance: 21-01-2021

I. Introduction

One of the most important materials whose properties have been studied in catalysis is the metallic oxide. Reducible and irreducible metallic oxides have a wide range of structural and morphological properties that make them excellent candidates for catalysts. They can act either as independent catalysts or can be functionalized through the dispersion of active components, such as metal nanoparticles. The study of the metal-oxide interface is very important in catalysis, mainly because each component has a significant effect on the catalyst's selectivity and activity. The catalytic reactivity and selectivity can be greatly influenced by both oxide and support characteristics, and also by the metal-support interaction[1].

The rigorous morphological control of the active sites on supported metal catalysts, as well as of the support's geometry, implies the design and the practical realization of a new advanced material architecture that significantly could enhance the reaction rate and the reaction selectivity[2,3]. The synthesis of nanoparticles with a controlled morphology and their dispersion on a support with a large BET-specific surface represent an advantageous way for controlling the composition and the size of the catalytic active phase. The study of nanoparticles with desired properties and controlled morphology has experienced impressive development over the last decade because of their huge potential in nanotechnology[4].

Many methods have been used for the synthesis of nanoparticles: i) sol-gel method[5]; ii) polyol method[6-8]; iii) hydrothermal synthesis[9] and iv) green synthesis method[10].

The nanoparticles (Nps) of noble metals Rh, Pd, Pt, Ru and of the transition metals like Co and Ni, have been identified as the active species for heterogenous catalysis. In many applications, the noble metal-based catalysts are too expensive to be used in a large scale. To diminish the costs, in practice, the metals are generally deposed on oxidic supports.

The polyol method is one of the most accessible ways of obtaining the nanoparticles, because the structure of the nanoparticles can be conveniently adjusted from the preparation stage, before their dispersion on the oxide support[11].

The catalysts physicochemical properties play a significant role in the catalytic performance. Porosity, surface area, the interaction between components, basicity, the capacity of oxygen storage and reducibility are the main characteristics of a catalyst. An appropriate selection of the support should be considered for its textural and chemical properties.

The basicity of supports is one of the important factors for certain catalytic reaction of hydrocarbon reaction. Thus, the basicity of support for dry reforming of methane reaction (DRM)[12] has a significant role in reducing the carbon formation.

Yide et al.[13] show that improving the surface basicity by promoting La_2O_3/ZnO catalysts in the oxidative coupling of methane reaction leads to the creation of active oxygen species, which manifests itself by the enhancing of the reactivity and CO_2-selectivity.

Gao et al. investigating controlled hydrothermal synthesis of MgO adsorbents under different reaction temperatures[14], noticed that CO_2 adsorption is associated with the generation of unsaturated oxygen sites, with defects and with the highly basic M–O–M ion pairs.

A significant contribution to the enhancement of the deactivation resistance in the decomposition of CH_4 can also be attributed to the increasing of the catalysts' basicity. Thus, the basic sites accelerate the activation of mildly acidic CO_2, that oxidizes the surface carbon. The presence of activated CO_2 on the catalyst surface inhibits the carbon formation[12].

The purpose of this work is the synthesis of stable Rh nanoparticles (Rh-Np) with a controlled morphology by the alkali polyol method, using the PVP and their assembly with different oxide support, and the morphological characterization of the surface catalysts (the geometry of the oxide support surface, basicity) through the prism of the fractal theory.

There are two major problems related to heterogenous catalysis and catalysts: it is hard to imagine that a catalyst is a sum of ideal, well-known pieces implied in simple phenomena and on the other hand, it is hard to model the changing of such a complicated object, which is the catalyst, during the chemical reaction. It is the role of the fractal theory to offer some answers on these challenges. From a geometric point of view, surface catalysts, its defects and irregularities are often self-similar, meaning that nanoparticles deposed on various substrates can be described in terms of fractal geometry[15,16]. Surfaces fractal dimensions take values between 2 and 3, with fractal dimension (D) equal or close to 2 for smooth surfaces and D close to 3 for highly irregular surfaces. There are a lot of methods to compute fractal dimension: from analyzing micrographs (TEM, AFM, STM) to neutron or X-Ray scattering or fitting the adsorption isotherm. Fractal theory was applied to describe the properties of the supported catalysts[17-20]. Catalysts are successful candidates to be described by fractal theory, as they are usually materials with higher BET area, very irregular, with a shape difficult to describe as a convolution of planar surfaces[16]. The fractal theory was used to describe nanoparticles and nanostructured agglomerates morphology, also[21-24].

The paper is focused on computing fractal dimensions of the oxides supports Al_2O_3, TiO_2, WO_3 and of Rh-nanoparticles deposed on the supports, using TEM micrographs analysis and the nitrogen adsorption-desorption isotherms analysis, the last method was used only in the case of Rh-Nps supported on oxides, before and after CO_2-Temperature Programmed Desorption. Results will be correlated with the total, weak, medium and strong basicity, obtained from CO_2-Temperature Programmed Desorption (TPD) profiles. Also, the samples will be characterized by X-ray powder diffraction, to characterize the morphology of Rh/oxide system and by CO pulse chemisorption to estimate the exposed rhodium surface area. The paper proposed an explanation concerning the strong dependence of the basicity on the fractal dimension, related to Rh encapsulation via SMSI.

II. Material And Methods

Preparation

Rh nanoparticles protected by polyvinyl pyrrolidone (PVP) were prepared by the modified alkaline polyol method. The preparation protocol, described in detail in a previous publication[1] , has been improved in order to obtain nanoparticles of the smallest size. Obtaining of highly dispersed particles on various supports

Rh/WO_3, Rh/TiO_2 and Rh/Al_2O_3 catalysts with metal loading 1%, by impregnation of the support powder with rhodium nanoparticle dispersed in water, is the aim of this study.

In a typical synthesis, 10 mL of 38 mM Rh(NO3)3 Wako (9%Rh) solution in ethylene glycol was added dropwise, with stirring of 100 mL alkaline solution 25 mM NaOH and polyvinyl pyrrolidone (PVP, Alfa Aesar) MW 8000, 38 mM (calculated in terms of the repeating units) held at 160 °C in hydrogen flow (25cm3/min) under vigorous stirring in a flask fitted with three necks. The alkaline polyol synthesis, ethylene glycol (EG) serves as both solvent and reducing agent while the PVP (polyvinyl pyrrolidone) acts as capping agent to avoid agglomeration. The temperature is maintained at 160 °C for 90 min to ensure the nucleation process and growing of the metallic particles, as the metallic precursor is totally reduced to metallic phase by ethylene glycol. The obtained suspension of the noble metal nanoparticles contains uniform particles with nanosized dimension. Then, the solutions were cooled to room temperature, keeping the inert atmosphere in the system.

The metallic nanoparticles were separated by the addition of an equivalent volume of acetone to the colloidal suspensions. Then, the mixture was cooled to -16 °C for 24 h; the precipitates were washed several times with acetone and separated by centrifugation at 12000 rpm to remove any traces of remained EG and PVP and afterward dried in oven at 100 °C for 6 h.

The Rh-support materials were obtained by dispersing the Rh nanoparticles, previously synthesized by sonication in water, on Al_2O_3 (γ –alumina, Aerosil, Japan) and TiO_2-P25 (Aerosil, Japan), WO_3 (Sigma Aldrich). The catalytic materials, Rh/support (Rh/Al_2O_3, Rh/TiO_2, Rh/WO_3) were dried at 100°C for 4 h and then calcined in air at 500°C for 2 h, to remove the PVP capping agent.

Preview work for pure PVP polymer shows water desorption below 200°C, but the total irreversible decomposition occurs at ~400°C. At the temperature >400°C, the polymer chains break and the radicals decompose into different fragments[25].

X-ray powder diffraction characterization

XRD measurements for Rh-Nps and Rh-Support were performed with Ultima IV X-Ray Diffractometer (Rigaku Japan) operated at 40 kV and 30mA using Cu Kα radiation (Kα = 1.54 Å) with a scan rate of 50C/min and 0.02° step size. The XRD diffractograms were collected between 10° and 80° (Fig. 1). XRD results indicate the formation of well dispersed and small size nanoparticles as it is discussed below.

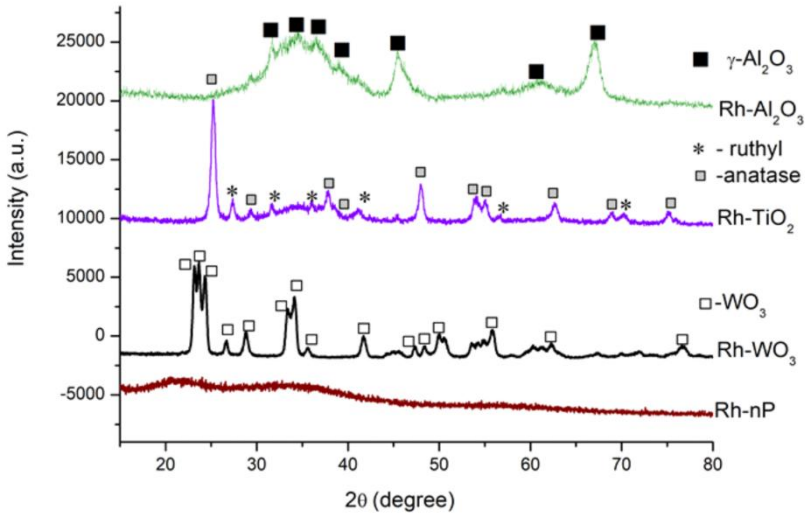

Fig. 1 XRD Spectra of Rh-Nps and of the Rh-Nps on different supports (Al_2O_3, TiO_2 and WO_3).

The absence of the characteristic XRD reflections for the Rh-Np supported on WO_3, TiO_2 and Al_2O_3 can be explained by the small size of Rh nanoparticles (d = 1.2-1.5 nm) and by the highly dispersion of Rh species on the support. For all samples, no sharp peaks for Rh-Np can be observed, indicating that Rh nanoparticles are well dispersed and their crystal sizes are very small, as observed in the TEM images. Sun et al.[26], using molecular dynamic simulation, demonstrates that the formation of amorphous structure is inevitable for metallic nanoparticles when reducing their diameter down to ≈ 1 nm. As expected, it is noticed that the supported catalysts show only the characteristic diffraction lines of oxides (WO_3, TiO_2 -anatase and -rutil, and γ-

Al_2O_3). To produce the characteristic XRD peaks, the crystalline structure should be at least few nanometers in size[27].

TEM electron microscopy

The TEM (Transmission Electron Microscopy) and HRTEM (High Resolution Transmission Electron Microscopy) characterization of catalysts was performed with FEI Tecnai G2-F30 S-Twin microscope operated at 300 kV. Small amount of the colloidal and supported Rh nanoparticles and Rh supported were drop-cast on holey carbon-coated copper grids and subsequently air-dried before TEM analysis (Fig. 2).

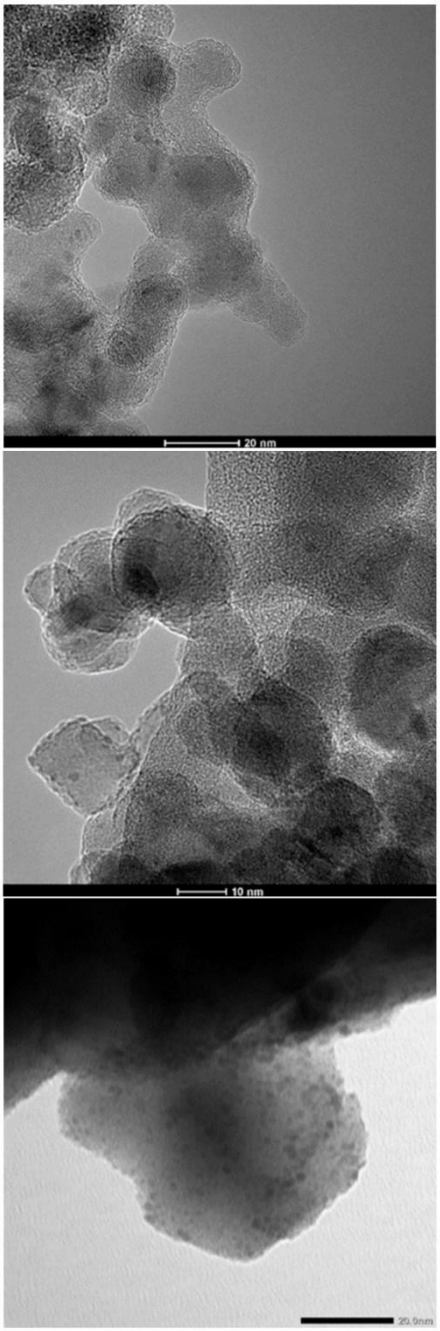

Fig. 2 TEM images from top to bottom: Rh/Al_2O_3, Rh/TiO_2, Rh/WO_3.

Nitrogen adsorption isotherms

Nitrogen adsorption isotherms were recorded at 77 K using a Micromeritics ASAP 2020 analyzer. Each sample was degassed at 250 ºC for 6 h under vacuum before analysis. The BET surface area was calculated

according to the Brunauer- Emmett-Teller (BET) equation, using adsorption data in the relative pressure range between 0.05 and 0.30.

The isotherms, depicted in Figs. 3 and 4, are type IV according to IUPAC classification, and show H3 hysteresis loop, that could be related to slit shape pores and capillary condensation in mesopores[28,29]. BET surface areas are presented in Table 1.

Table no 1 BET surface areas, particle sizes, metal surface area and nanoparticles dispersion for Rh/Al_2O_3, Rh/TiO_2 and Rh/WO_3.

Sample	Dispersion (%)	Particle size (nm)	Metal surface area (m^2/g)	BET Surface Area (m^2/g) (before TPD)	BET Surface Area (m^2/g) (after TPD)
Rh/Al_2O_3	34.83	1.12	1.36	97.2	98.5
Rh/TiO_2	19.73	1.93	0.88	56.9	47.1
Rh/WO_3	22.76	1.63	0.98	27.32	25.5

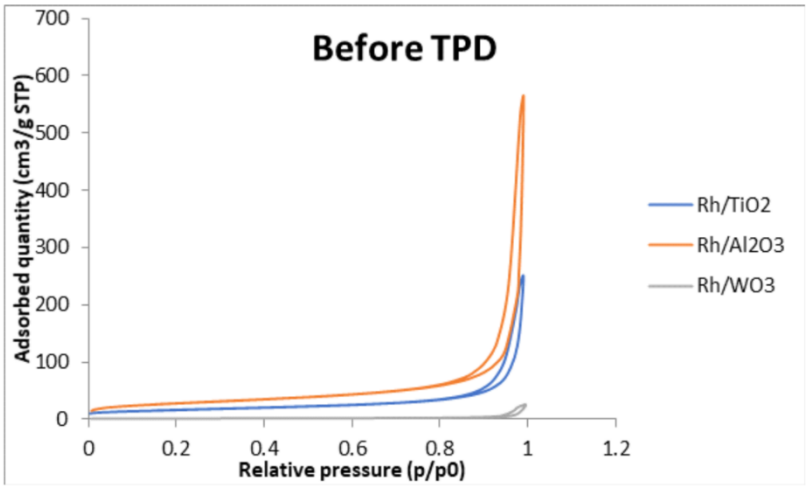

Fig. 3 Nitrogen adsorption – desorption isotherms before CO_2- TPD.

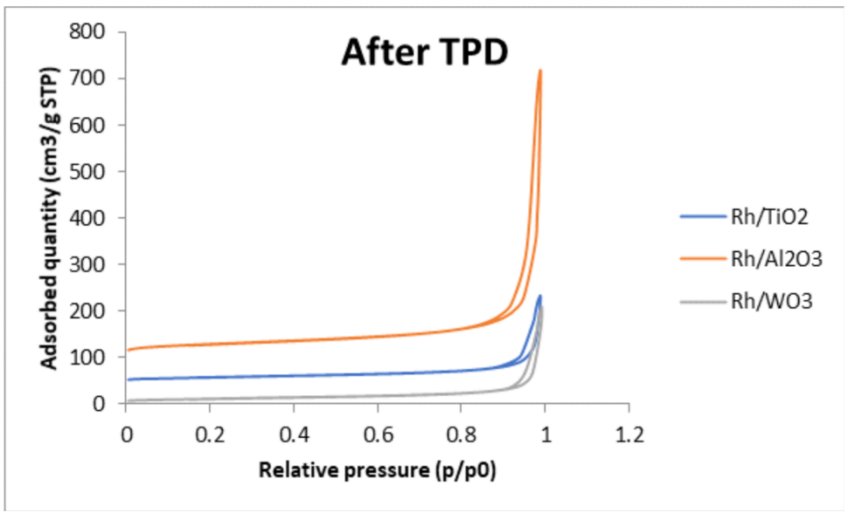

Fig. 4 Nitrogen adsorption – desorption isotherms after CO_2- TPD (Rh/TiO_2 and Rh/Al_2O_3 isotherms were shifted).

CO pulse chemisorption

The exposed rhodium surface area was estimated by CO pulse chemisorption performed at room temperature using a ChemBet-3000 Quantachrome Instrument equipped with a thermal conductivity detector (TCD). Prior to CO chemisorption measurements, the catalytic materials Rh/Al_2O_3, Rh/TiO_2 and Rh/WO_3 were reduced with H_2 at 400°C for 1 h and then cooled to room temperature in inert gas (He). The chemisorption amount of CO was directly correlated to the amount of exposed Rh sites on the catalysts' surface.

As can be seen from Table 1, the dispersion of the rhodium nanoparticles on the support surface varies in the order $Rh/TiO_2<Rh/WO_3<Rh/Al_2O_3$. In the case of Rh/TiO2, the dispersion is smaller than in the case of the other samples. This fact can be explained by the encapsulation of Rh nanoparticles by support oxide. Previous studies have hypothesized that the encapsulation of Rh crystallites probably occurs as an effect of a simple thermal treatment, especially for the 1-2 nm crystallites[30].

The differences in Rh nanoparticle size estimates from CO chemisorption and TEM image may have resulted due to a possible presence of a fraction of small particles accessible to the gas phase, but not detectable by TEM techniques. The size estimated from CO chemisorptions was significantly larger compared to that determined by TEM techniques[31].

CO_2 – Temperature Programmed Desorption (CO_2-TPD)

CO_2-TPD profiles of the Rh-supported catalysts were carried out to investigate the distribution of basic sites on surfaces of the Rh/Al_2O_3, Rh/WO_3 and Rh/TiO_2 (Fig. 5). The characteristic peaks of Rh-supported materials, corresponding to the desorption temperatures of CO_2, signify the base strength of the Rh-supported samples, meanwhile the area under the profile curves gives the amount of the basic sites[32].

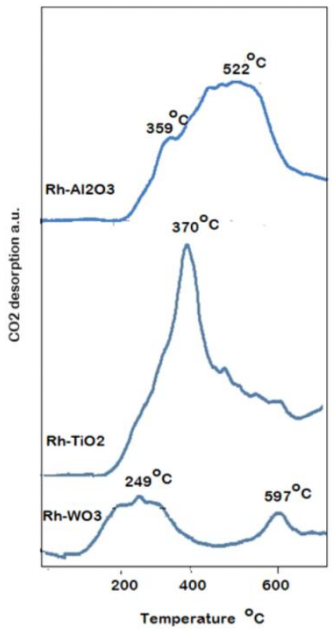

Fig. 5 The quantitative distribution of the basic sites on the surface on $Rh-WO_3$, $Rh-TiO_2$ and $Rh-Al_2O_3$.

Depending on the CO_2 desorption temperature, three types of basic centers are distinguished, exhibiting different thermal stability. Boukha et al.[31] reported that the deposition of Rh on various supports influences both the amount of adsorbed species and their stability.

Gao et al.[14] performed in situ DRIFTS measurements to investigate the species produced and adsorbed on the MgO adsorbent surface during interaction with CO_2. They evidenced three carbonate species formed on basic oxides: bicarbonate, bidentate and unidentate carbonates. Also, the basic strength of O_2^- was correlated with the coordination number and electronegativity of the coordination metal ions[14].

The desorption of CO_2 at low temperatures in the range 100-200°C is associated with weak basic sites. The CO_2 adsorbed on the surface forms superficial, weak bonds with the HO^- groups that result in the generation of bicarbonate species, characterized by the C–OH bending mode of bicarbonate species containing surface hydroxyl groups and by the symmetric stretch O-C-O of bicarbonates[33].

In the region of 200°C –400°C the medium-strength basic sites were assigned to the acid-base Lewis pairs with formation of bidentate carbonate, evidenced by the asymmetric stretch O–C–O of bidentate carbonate species[14]. Metal oxide with lower coordinated O_2^- and lower electronegative metal ions exhibited stronger basic strength[34].

The strong and very strong basic sites, over 400°C, are correlated with the formation of unidentate carbonate species during the carbonation with CO_2, as a result of strong metal-support interaction (SMSI). Ding et al[35] suggest the existence of symmetric and asymmetric O-C-O stretch of unidentate carbonates. The adsorption of the different carbonate species on a fractal surface is schematic represented in Fig. 6. The fractal surface was simulated using the Takagi equation[36] with D=2.26.

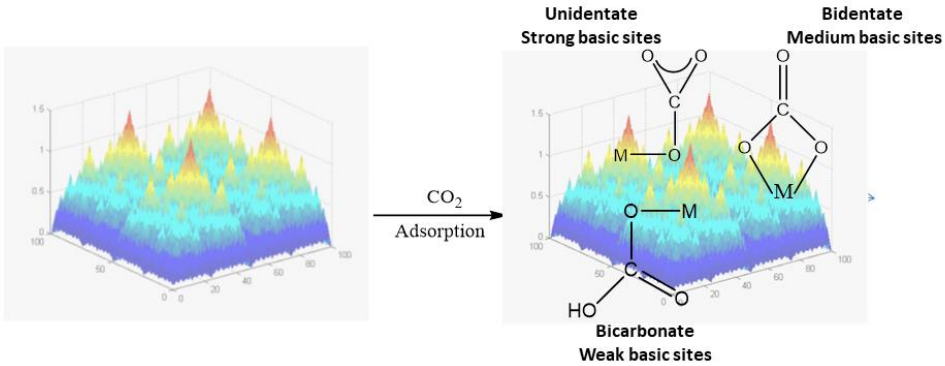

Fig. 6 Schematic illustration of the basic sites on a fractal surface (Takagi simulated fractal surface[36]).

The Rh-WO_3 sample exhibits two peaks: one at 249 °C, corresponding to low and medium-strength basic sites, and another at 597 °C, corresponding to strong basic sites.

The profile of the Rh-TiO_2 sample is characterized by a sharp peak below 370°C and a wide plateau over 400°C, which are assigned to medium and very strong basic sites, respectively, meanwhile the Rh-Al_2O_3 sample exhibits two peaks centered at 359 °C and 522 °C, corresponding to moderate and strong basic sites, respectively.

The quantification of desorbed CO_2 for all catalysts is included in Table 2. These values were obtained by integrating the area below the CO_2 desorption curve for each sample, using known CO_2 calibration date and assuming that only one CO_2 molecule can adsorb on a single site.

The intensity of the CO_2 desorption peaks have changed as the nature of support was changing.

The total basicity of these materials increases in the following order: the total number of basic sites of Rh-WO_3 (370 µmol g^{-1}) < Rh-TiO_2(805 µmol g^{-1}) < Rh-Al_2O_3 (990 µmol g^{-1}).

Table no 2 The quantification of desorbed CO_2 for Rh/Al_2O_3, Rh/TiO_2 and Rh/WO_3

Catalyst	Weak basic sites* µmol CO_2g^{-1}	Medium basic sites* µmol CO_2g^{-1}	Strong basic sites* µmol CO_2g^{-1}	Total surface basicity, µmol CO_2g^{-1}	Surface basicity, µmol CO_2m^{-2}	Weak basic sites, %	Medium basic sites, %	Strong basic sites, %
Rh/Al_2O_3	4.12	35.25	970.7	990.10	10.11	0.41	3.56	96.02
Rh/TiO_2	9.64	89.70	706.20	805.55	16.78	1.19	11.13	87.66
Rh/WO_3	74.59	90.65	105.73	270.98	9.74	20.10	24.43	55.45

* These values were obtained by integrating the area below the CO_2 desorption curve for each samples and using a known CO_2 calibration peak.

TEM analysis for computing fractal dimension

TEM micrographs were investigated using the correlation function method[37] and the variable length scale method[38].

The correlation function method uses the average of the height correlation function:

$$G(p,q) \equiv < [h(x,y) - h(x+p, y+q)]^2 >_{x,y},\ r = \sqrt{(x^2+y^2)} \qquad (1)$$

where h(x,y) is the height at the (x,y) coordinates, obtained as the grey level of each pixel,$<>_{x,y}$ is the average of the correlation function over x and y. The height correlation function scales as:

$$G(r) \sim r^{2\alpha}, r << L, \quad (2)$$

where $\alpha=3 - D$, and D is the fractal dimension. The log-log representation of Eq. (2) leads to the fractal dimension determination.

The variable length scale method was proposed by Chauvy et al[38] and consists of computing the surface roughness $R_{q\varepsilon}$, averaged over each box of linear size ε, roughness which scales with ε as:

$$R_{q\varepsilon} \sim \varepsilon^{3-D}, \quad (3)$$

where D is the fractal dimension.

Adsorption isotherm method for computing fractal dimension

Avnir and Jaroniec[39] developed a method to compute the fractal dimension of catalysts using the Dubinin approach[40]. They integrated the Dubinin isotherm in the region of $p/p_0 = 0.05$ to the micropore filling pressures, obtaining for microporous solids the following equation:

$$\theta = \frac{1}{2} C \Gamma\left(\frac{3-D}{2}\right) m^{-(D-3)/2} A^{-(3-D)} \quad (4)$$

where Γ is the gamma function, C and m are constants, D is the fractal dimension, and $A = RT\ln(p_0/p)$ is the adsorption potential, or, in a more condensed manner:

$$\theta = K\left[\ln\left(\frac{p_0}{p}\right)\right]^{-(3-D)} \quad (5)$$

which can be used to fit experimental data and to compute fractal dimension.

Equation (5) is valid for the capillary condensation regime, when the liquid-gas surface tension forces control the interface.

For the polymolecular regime of the generalized Frenkel-Halsey-Hill equation, Eq. (5) becomes:

$$\theta = K[\ln\left(\frac{p_0}{p}\right)]^{-\frac{3-D}{3}} \quad (6)$$

Equations (5) and (6) can be written in a compact form as[41]:

$$\theta = K[\ln\left(\frac{p_0}{p}\right)]^{-\frac{1}{m}} \quad (7)$$

where $m = \frac{3}{3-D} \quad for \ m > 3 \ and \quad m = \frac{1}{3-D} \quad for \quad m < 3.$

D is the surface/pore fractal dimension of the solid, m>3 characterizes the FHH regime in which the dominant force is the substrate potential and m<3 characterizes the capillary condensation regime, where the liquid-gas surface tension forces control the interface[41].

III. Result

Fractal dimensions computed from TEM micrographs

Some TEM micrographs of the samples were presented in Fig. 2. In order to analyze them, the images were prepared to enhance the contrast by improving the image histogram to avoid clipping[42]. For every sample, 5 images, at different magnifiers were analysis. Results are presented in Table 3.

Table no 3 Fractal dimensions (before TPD, fresh samples) from TEM micrographs of Rh-Np/support samples and of the support samples; "cor" means fractal dimension obtained using the correlation function method (Eqs. 1 and 2) and "vls" means fractal dimension computed using the variable length scale method (Eq.3).

Sample	Fractal dimension	Correlation coefficient	Self-similarity domain (nm)
Rh/Al_2O_3	2.872±0.001 (cor) 2.784±0.051 (vls)	0.9910 0.8186	4.4-14.4 7.2-11.8
Al_2O_3	2.952±0.001 (cor) 2.962±0.004(vls)	0.9375 0.9549	0.7-8.1 1.4-2.8
Rh/TiO_2	2.733±0.001 (cor) 2.832±0.009 (vls)	0.9884 0.9649	4.9-14.4 5.4-17.3
TiO_2	2.831±0.001 (cor) 2.911±0.017 (vls)	0.857 0.925	6.5-11 2.4-3.00
Rh/WO_3	2.490±0.001 (cor) 2.330±0.001 (cor) 2.469±0.035 (vls) 2.226±0.047 (vls)	0.9975 0.9991 0.9747 0.9334	0.2-2.7 2.7-13.8 4.5-11 11-29.3
WO_3	2.660±0.004 (cor) 2.293±0.002 (cor) 2.652±0.042 (vls)	0.990 0.986 0.949	0.2-1.2 1.8-5.0 4.1-5.9

All samples exhibit strong fractal properties, both methods indicating self-similarity over a large domain.

The addition of Rh nanoparticles onto Al_2O_3, TiO_2 and WO_3 supports tends to decrease the fractal dimension of the Rh/support system. Therefore, the fractal dimension of Al_2O_3 support is around 2.95-2.96, higher than the fractal dimension of the Rh/Al_2O_3 catalyst; the fractal dimension of the Rh/TiO_2 takes values in the range 2.73-2.83, meanwhile the support exhibits a higher fractal dimension of 2.83-2.91. Decreasing of fractal dimension when Rh-Np is added can be explained by the blockage of the surface pores and irregularities by Rh-nanoparticles or/and by Rh encapsulation via SMSI (strong metal-support interaction)[16].

WO_3 support has a bi-modal fractal behavior characterized by a fractal dimension of 2.65-2.66 and another fractal dimension, of a superposed structure, of 2.29. Adding Rh-nanoparticles on the WO_3 surface, the support fractal dimension of 2.65-2.66 is lowered to 2.46-2.49 as an effect of nanoparticles, meanwhile the other characteristic fractal dimension is found between 2.22-2.33.

Fractal dimensions computed from DR isotherms before TPD (fresh samples)

Log-log curves of adsorption coverage over logarithm of pressure ratio (Fig. 7) indicate values of m parameter below 3, meaning that the samples are in the capillary condensation regime, following that the fitting equation is the Dubinin-Radushkevitch (DR) fractal isotherm[43].

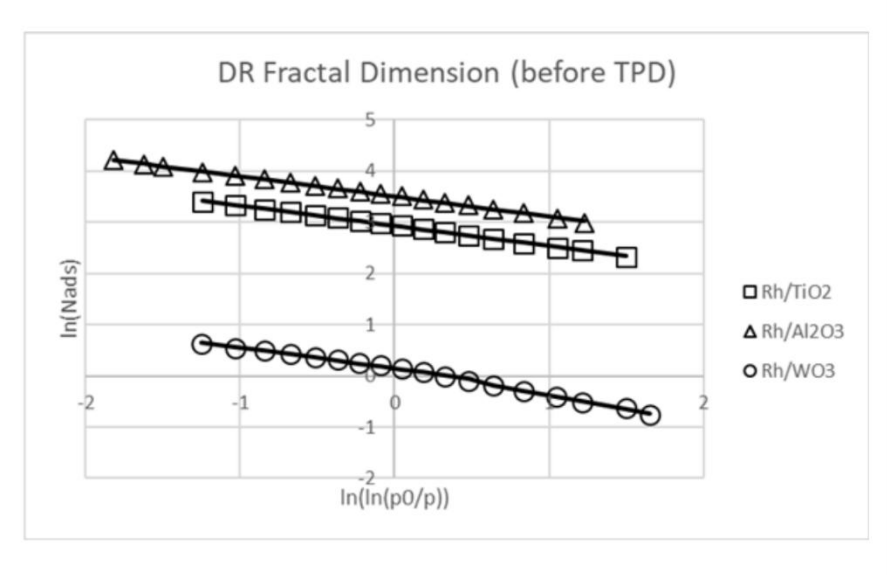

Fig. 7 The fractal dimension determination from BET isotherms using DR equation (before TPD).

Fractal dimensions, computed using the DR equation, are presented in the Table below (Table 4).

Table no 4 Fractal dimensions (before TPD) computed from DR fitting isotherms

Sample	Fractal dimension	Correlation coefficient	Self-similarity domain (p/p_0)	m
Rh/Al_2O_3	2.607±0.004	0.9986	0.033-0.850	2.54
Rh/TiO_2	2.604±0.003	0.9989	0.011-0.750	2.52
Rh/WO_3	2.448±0.012 2.589±0.014	0.9977 0.9889	0.005-0.200 0.200-0.750	1.81 2.43

DR fractal dimensions are lower than the TEM fractal dimensions for all samples, except for Rh/WO_3, where a bi-modal behavior is emphasized. DR fractal dimension shows the filling capacity of the pores-system, meanwhile TEM fractal dimensions characterize the sample surface as it is seen in TEM micrographs. From this point of view, TEM fractal dimension measures correlations and similarities between points on the surface, meanwhile DR fractal dimension measures the fractal distribution of pores.

The last sample, Rh/WO_3, which exhibits a fractal behavior characterized by two-superposed fractal structures in the TEM images, emphasizes the same behavior of the DR fractal dimensions.

Fractal dimensions computed from DR isotherms after TPD

After TPD, all catalysts exhibit two-superposed fractal structures (Fig. 8, Table 5). Rh/TiO_2 is characterized by two fractal dimensions: 2.29 (the fractal dimension of Rh-Nps set) and 2.54 (the fractal dimension of the porous

substrate of TiO_2). Rh/Al_2O_3 and Rh/WO_3 exhibit higher fractal dimensions: 2.53, respectively 2.59 (Rh-Np set) and 2.62 and 2.66, respectively (the porous substrate).

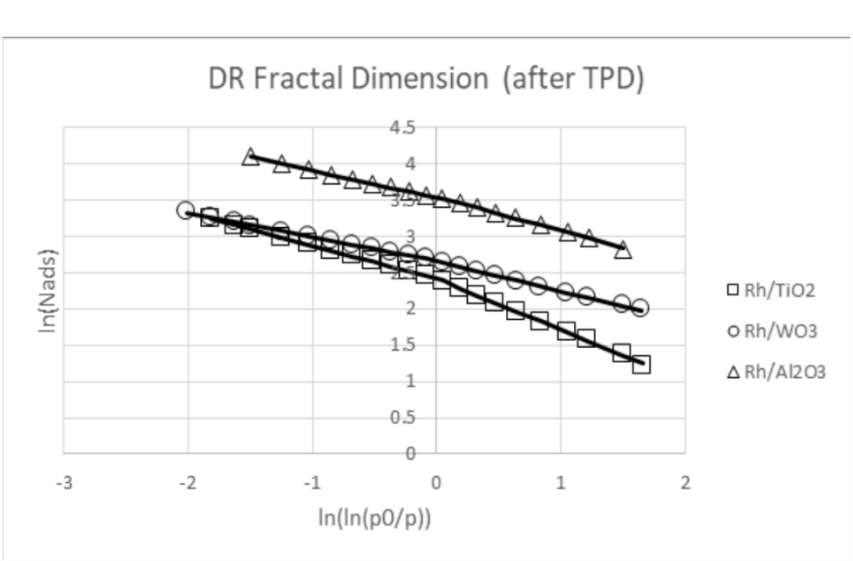

Fig. 8 The fractal dimension determination from BET isotherms using DR equation (after TPD).

Table no 5 Fractal dimensions (after TPD) computed from DR fitting isotherms

Sample	Fractal dimension	Correlation coefficient	Self-similarity domain (p/p_0)	m
Rh/Al_2O_3	2.534±0.009 2.623±0.002	0.9973 0.9998	0.011-0.350 0.350-0.800	2.14 2.65
Rh/TiO_2	2.292±0.011 2.548±0.005	0.9980 0.9987	0.005-0.350 0.350-0.850	1.41 2.21
Rh/WO_3	2.595±0.008 2.668±0.003	0.9970 0.9993	0.005-0.350 0.350-0.875	2.47 3.01

To notice the m-value of 3.01 for the last fractal structure, higher than 3, meaning that Rh/WO_3 is in the limit of the capillary regime and it could be treated also as a surface, not a porous, interconnected system[41,44].

Fitting Rh/WO_3 isotherm with fractal FHH equation, in which the dominant force is the substrate potential (Fig. 8), the fractal dimension for the 0.350-0.875 interval becomes 2.003±0.003. It seems that the thermal treatment (TPD) induces surface reorganization and restructuration which modify the self-similarity of the samples, reducing surface correlations and ordering onto catalyst surface, lowering the fractal dimension.

The fractal dimensions after TPD (thermal treatment) decrease for Rh/Al_2O_3 and Rh/TiO_2 also, indicating possible Rh encapsulation occurring at high temperature, related to higher values of strong basicity sites of Rh/Al_2O_3 and Rh/TiO_2, as we shall discuss below.

IV. Discussion

The low and medium basic sites number exhibits a slow decrease with both TEM fractal dimension of Rh supported on oxides (Fig. 9) and TEM fractal dimension of the oxide support (Fig. 10), meanwhile the number of the total basic sites and the number of the strong basic sites increase with TEM fractal dimension (Fig. 11 and Fig. 12). The same behavior is emphasized by DR fractal dimension before TPD (fresh samples) (Fig. 13 and Fig. 14) and after TPD (Fig. 15). These behaviors lead to the conclusion that there is a strong dependence between the basic sites` distribution and the fractal properties of the catalysts. Higher fractal dimensions favor strong basic sites, as Rh/Al_2O_3 and Rh/TiO_2 catalysts exhibit, meanwhile lower fractal dimensions favor low and medium basic sites, as for Rh/WO_3 catalyst.

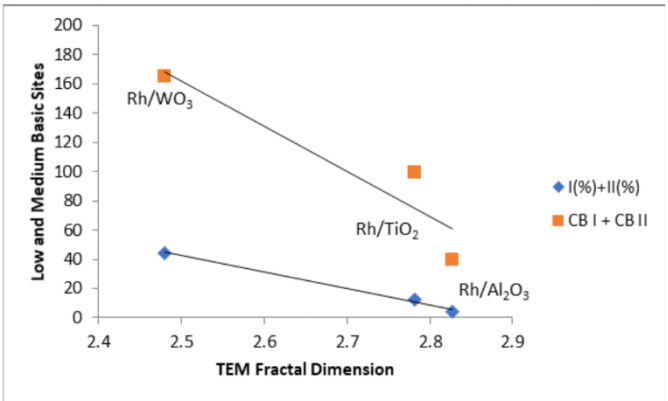

Fig. 9 Low and medium basic sites versus TEM fractal dimension of Rh supported on oxides.

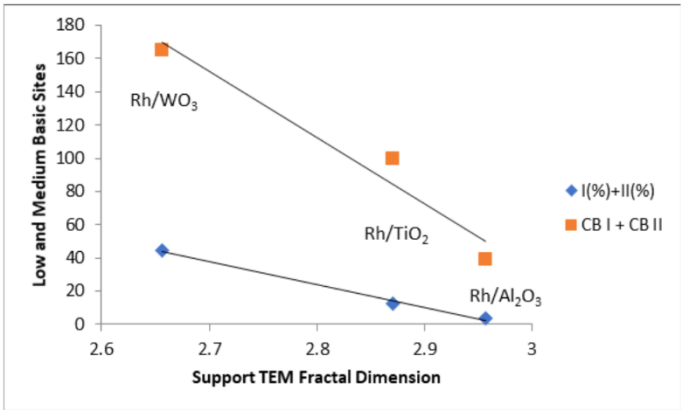

Fig. 10 Low and medium basic sites versus support TEM fractal dimension.

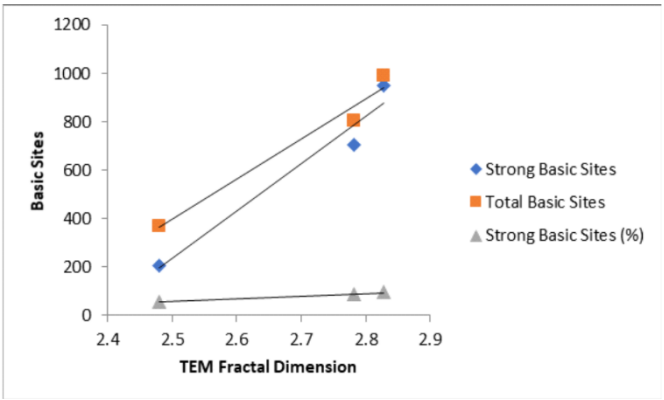

Fig. 11 Total and strong basic sites versus TEM fractal dimension of Rh supported on oxides.

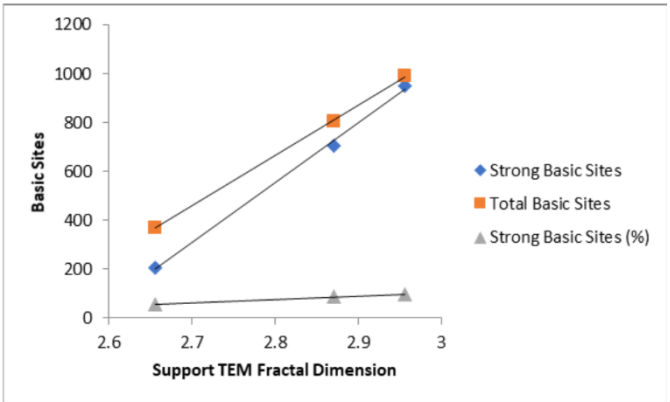

Fig. 12 Total and strong basic sites versus support TEM fractal dimension.

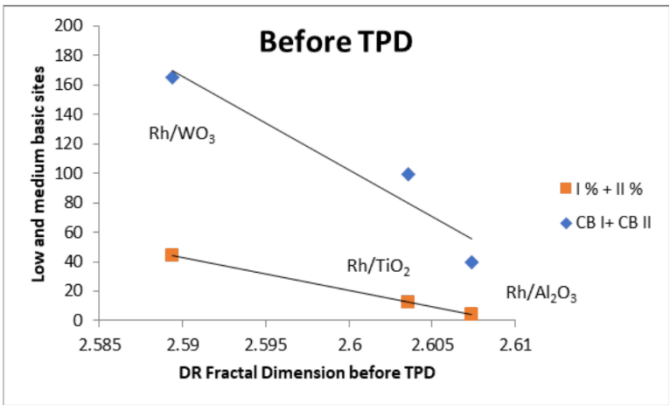

Fig. 13 Low and medium basic sites versus catalysts' DR fractal dimension, before TPD.

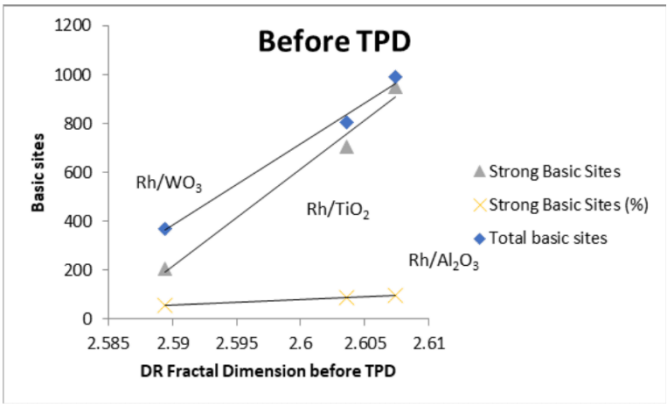

Fig. 14 Total and strong basic sites versus catalysts' DR fractal dimension, before TPD.

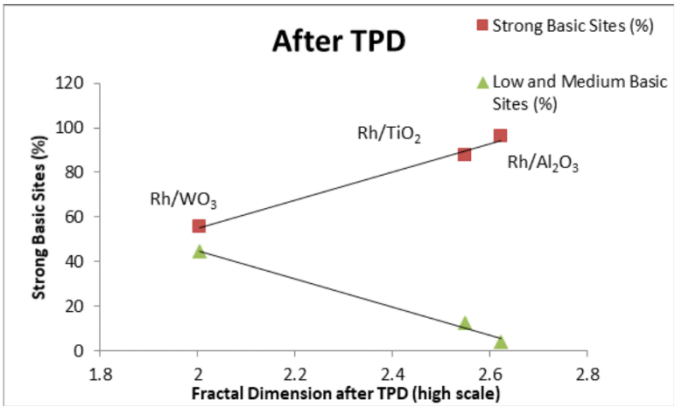

Fig. 15 Strong basic sites percentage share and low and medium basic sites percentage share after TPD versus fractal dimension (high scale); fractal dimensions are computed using DR equation for Rh/TiO_2 and Rh/Al_2O_3 and FHH equation for Rh/WO_3.

The number of strong basic sites, assigned to low-coordinated O^{2-}, increases with fractal dimension as a result of higher roughness/porosity of the support, favorizing SMSI (strong metal support interactions) via encapsulation of Rh at higher temperature and, therefore, oxide migration on top of the metal nanoparticles, leading to monodentate carbonate, as it happens in Rh/Al_2O_3 and Rh/TiO_2 catalysts. It seems that the higher is the surface fractal dimension, therefore surface porosity, the higher is the number of encapsulation processes of Rh-nanoparticles on the support, leading to a higher strong basicity. Surface inhomogeneities leading to higher fractal dimensions (defects, vacancies, fractures, pores) encourage SMSI and, therefore Rh encapsulation. It is important to notice that the number of strong basic sites is higher as TEM fractal dimension is higher, meaning that surface inhomogeneities are high and an interconnected porous system is present; the number of strong basic sites is, also, higher as DR fractal dimension after TPD (after the thermal treatment) is higher, after more Rh-encapsulation processes and surface reconstruction/restructuration take place.

On the other hand, weak and medium basic sites, ussually assigned to CO_2 physisorption, to superficial HO^- groups forming bicarbonate species with CO_2 or to acid-base Lewis pairs leading to bidentate carbonate, are important when fractal dimension is lower, with less defects, vacancies, pores. In the case of alumina, heat treatment causes a substantial decrease in the number of surface HO^- groups, meaning that the basic sites involving HO^- groups will occur only to 300-400^oC, decreasing at higher temperature[45]**.** As we already noticed from computing the fractal dimension after TPD, the temperature increasing will induce, also, a lowering of the fractal dimension over a self-similarity domain of pressure, which can be correlated, probably, with the decreasing of the number of HO^- groups.

In the case of Rh/WO_3, weak and medium basic sites have a high contribution to basicity, 20.10% and 24.43%, respectively, in correlation with lower fractal dimensions of the catalyst. After thermal treatment occurring in TPD measurements, at higher pressure, the surface move from capillary condensation regime to the FHH regime in which the dominant force is the substrate potential, meaning that surface reconstruction/restructuration occurs.

Enhancing catalytic activity for DRM of Rh/Al_2O_3, Rh/TiO_2 and Rh/WO_3 implies higher basic sites number, as literature showed[12,46]. A method to achieve this is to use supports with higher fractal dimension; in this situation, even if, by adding nanoparticles, such as Rh, the catalyst fractal dimension will be lowered by encapsulation, the fractal dimension will be high enough to favor strong basicity sites formation via Rh encapsulation, as a consequence of strong metal-support interaction (SMSI).

V. Conclusion

The purpose of this work is the synthesis of the morphological-controlled Rh nanoparticles (Rh-Np) by the alkali polyol method, their assembly with different oxide supports, and surface characterization of the catalysts through the prism of the fractal theory. Also, the samples were characterized by X-ray powder diffraction, to characterize the morphology of Rh/oxide system and by CO pulse chemisorption to estimate the exposed rhodium surface area. TEM micrographs and the nitrogen adsorption-desorption isotherms were used to compute the fractal dimensions of Rh-nanoparticles supported on different oxides. The fractal properties were correlated with basicity computed from CO_2-Temperature Programmed Desorption (TPD) profiles.
Some conclusions are to be made:

- Fractal dimensions of Rh/Al_2O_3, Rh/TiO_2 and Rh/WO_3 were computed using TEM images analysis and nitrogen adsorption isotherms, before and after CO_2-Temperature Programmed Desorption; strong self-similarity properties were emphasized; fractal dimensions of TEM images of oxides supports Al_2O_3, TiO_2 and WO_3 were also computed;
- TEM analysis by fractal theory have revealed that adding Rh-nanoparticles on supports will decrease the system fractal dimension as a result of Rh encapsulation via SMSI (as in the case of Rh/Al_2O_3 and Rh/TiO_2 catalysts) or/and of the blockage of the pores/surface defects by Rh-nanoparticles.
- CO_2-TPD was used to compute the number of weak, medium and strong basic sites of the catalysts; there is a strong relation between basicity and fractal dimension;
- Meanwhile the number of weak and medium basic sites decrease as the fractal dimension increases, the number of strong and of the total basic sites increase as the surface fractal dimension increases.
- The number of strong basic sites, assigned to low-coordinated O^{2-} , increases with fractal dimension as a result of higher roughness/porosity of the support favorizing SMSI (strong metal support interactions) via encapsulation of Rh at higher temperature and, therefore, oxide migration on top of metal nanoparticles, leading to monodentate carbonate.
- Increasing the temperature while measuring the amount of CO_2 desorbed, will lower the fractal dimension of Rh/Al_2O_3 and Rh/TiO_2 as a result of Rh –encapsulation and surface restructuration; it is not the case of Rh/WO_3: even if the fractal dimension increases, this behavior cannot be assigned to Rh encapsulation and SMSI, but to the blockage of the surface pores and irregularities by surface restructuring.
- Weak and medium basic sites, ussually assigned to CO_2 physisorption, to superficial HO^- groups forming bicarbonate species with CO_2 or to acid-base Lewis pairs leading to bidentate carbonate are important when fractal dimension is lower as for Rh/WO_3 catalyst.

The further purpose of our work is to obtain enhanced catalytic activity for DRM of Rh/Al_2O_3, Rh/TiO_2 and Rh/WO_3: the first step was to prepare catalysts with higher fractal dimension of the oxide support, leading to higher fractal dimension of Rh/support, leading to Rh-encapsulation via SMSI, which improves nanoparticles dispersion on surfaces and leads to higher basicity sites number. Enhancing catalytic activity for DRM of Rh/Al_2O_3, Rh/TiO_2 and Rh/WO_3 implies higher basic sites number, and a method to achieve this is to use supports with higher fractal dimension; the paper proved that even if, by adding nanoparticles, such as Rh, the catalyst fractal dimension will be lowered by encapsulation, the fractal dimension will be high enough to favor strong basicity sites formation via Rh encapsulation, as a consequence of strong metal-support interaction (SMSI). The fractal theory proved to be a useful tool to emphasize both geometrical properties of the catalysts, but also, to bring clues about nanoparticles encapsulation and surface basicity.

Acknowledgements

Support of the project PCCDI/46/2018 MALASENT is gratefully acknowledged.

References

[1]. State R, Scurtu M, Miyazaki A, Papa F, Atkinson I, Munteanu C, Balint I, Influence of metal-support interaction on nitrate hydrogenation over Rh and Rh-Cu nanoparticles dispersed on Al_2O_3 and TiO_2 supports, Arabian Journal of Chemistry 2017;10: 975-984.
[2]. Holewinski A, Idrobo J-C, Linic S, High-performance Ag–Co alloy catalysts for electrochemical oxygen reduction, Nat. Chem. 2014; 6 :828–834.
[3]. Matsubu JC, Yang VN, Christopher P, Isolated Metal Active Site Concentration and Stability Control Catalytic CO_2 Reduction Selectivity, J. Am. Chem. Soc. 2015;137:3076– 3084.
[4]. Salata O, Applications of nanoparticles in biology and medicine, J Nanobiotechnology 2004;2(1):3. https://doi:10.1186/1477-3155-2-3.
[5]. Owens GJ, Singh RK, Foroutan F, Alqaysi M, Han CM, Mahapatra C, Kim HW, Knowles JC, Sol–gel based materials for biomedical applications, Prog. Mater. Sci. 2016;77:1-79.
[6]. Kim D, Jeong S, Moon J, Synthesis of silver nanoparticles using the polyol process and the influence of precursor injection, Nanotechnology 2006;17:4019-4024.
[7]. Papa F, Negrila C, Miyazaki A, Balint I, Morphology and chemical state of PVP-protected Pt, Pt–Cu, and Pt–Ag nanoparticles prepared by alkaline polyol method, J. Nanopart. Res. 2011;13:5057–5064.
[8]. Malik MA, Wani MY, Hashim MA, Microemulsion method: a novel route to synthesize organic and inorganic nanomaterials, Arab. J. Chem. 2012;5:397-417.
[9]. Darr JA, Poliakoff M, New Directions in Inorganic and Metal Organic Coordination Chemistry in Supercritical Fluids, Chem. Rev. 1999;99:495–542.
[10]. Gowramma B, Keerthi U, Mokula R, Rao DM, Biogenic silver nanoparticles production and characterization from native stain of Corynebacterium species and its antimicrobial activity, Biotech. 2015;5:195-201.
[11]. Koczkur MK, Mourdikoudis S, Polavarapu L, Skrabalak SE, Polyvinylpyrrolidone (PVP) in nanoparticle synthesis, Dalton Trans. 2015 ;44:17883-17905.
[12]. Jang W, Shim J, Kim H, Yoo S, Roh H, A review on dry reforming of methane in aspect of catalytic properties, Catalysis Today 2019; 324:15-26.

[13]. Yide X, Lin Y, Xiexian G, Effect of basicity and adding CO_2 in the feed on the oxidative coupling of methane over K_2O and SrO promoted La_zO_3/ZnO catalysts, Applied Catalysis A: General 1997;164:47-57.
[14]. Gao W, Zhou T, Wang Q, Controlled synthesis of MgO with diverse basic sites and its CO_2 capture mechanism under different adsorption conditions, Chemical Engineering Journal 2018;336:710–720.
[15]. Mandelbrot BB, The Fractal Geometry of Nature (Freeman, San Francisco, 1982).
[16]. Rothschild WG, Fractals in Heterogeneous Catalysis, Catalysis Reviews: Science and Engineering 1991;33(1-2):71-107.
[17]. Avnir D, Farin D, Pfeifer P, Molecular Fractal Surfaces, Nature 1984;308:261-263.
[18]. Dobrescu G, Rusu M, Vass M, Computer Simulations of Fractal Surfaces: Application in Adsorption, Fractals, 1993;1(3):430-438.
[19]. Coppens M-O, Froment GF, The Effectiveness of Mass Fractal Catalysts, Fractals, 1997;5(3):493-505.
[20]. Luque JJ, Gomez A, Cordoba A, Multifractal analysis of adsorbate in a catalyzed surface reaction, Fractals 2004;12(02):171-177.
[21]. Dobrescu G, Papa F, State R, Fangli I, Balint I, Particle size distribution of Pt–Cu bimetallic nanoparticles by fractal analysis, Powder Technology 2015;269:532-540.
[22]. Dobrescu G, Papa F, State R, Balint I, Characterization of bimetallic nanoparticles by fractal analysis, Powder Technology 2018;338: 905-914.
[23]. Kanniah V, Wu P, Mandzy N, Grulke EA, Fractal analysis as a complimentary technique for characterizing nanoparticle size distributions, Powder Technology 2012;226:189-198.
[24]. Ibaseta N, Biscans B, Fractal dimension of fumed silica: Comparison of light scattering and electron microscope methods , Powder Technology 2010;203:206-210.
[25]. Miguel-García I, Berenguer-Murcia A, García T, Cazorla-Amorós D, Effect of the aging time of PVP coated palladium nanoparticles colloidal suspensions on their catalytic activity in the preferential oxidation of CO, Catalysis Today 2012;187:2-9.
[26]. Sun Y, Zhuang L, Lu J, Hong X, Liu P, Collapse in Crystalline Structure and Decline in Catalytic Activity of Pt Nanoparticles on Reducing Particle Size to 1 nm, J. Am. Chem. Soc. 2007;129:15465-15467.
[27]. Peng J, Wang S, Performance and characterization of supported metal catalysts for complete oxidation of formaldehyde at low temperatures, Appl. Catal. B 2007;73:282-291.
[28]. Lowell S, Shields JE, Thomas MA, Thommes M, Characterization of Porous Solids and Powders Surface Area, Pore Size and Density, Particle Technology Series (Springer, Dordrecht, 2004).
[29]. Sing KSW, Williams RT, Physisorption Hysteresis Loops and the Characterization of Nanoporous Materials, Adsorption Science & Technology 2004;22:773-782.
[30]. Berko A, Ulrych I, Prince KC, Encapsulation of Rh Nanoparticles Supported on TiO_2(110)-(1 × 1) Surface: XPS and STM Studies, J. Phys. Chem. B 1998;102:3379-3386.
[31]. Boukha Z, Gil-Calvo M, de Rivas B, González-Velasco JR, Gutiérrez-Ortiz JI, López-Fonseca R, Behaviour of Rh supported on hydroxyapatite catalysts in partial oxidation and steam reforming of methane: On the role of the speciation of the Rh particles, Applied Catalysis A: General 2018;556:191-203.
[32]. Ivan SB, Fechete I, Papa F, Marcu IC, Ethane oxydehydrogenation over TiP_2O_7-supported NiO catalysts, Catalysis Today (2020) in press. https://doi.org/10.1016/ j.cattod.2020.02.005.
[33]. Baltrusaitis J, Schuttlefield J, Zeitler E, Grassian VH, Carbon dioxide adsorption on oxide nanoparticle surfaces, Chemical Engineering Journal 2011;170:471-481.
[34]. Jiao X, Li L, Zhao N, Xiao F, Wei W, Synthesis and Low-Temperature CO_2 Capture Properties of a Novel Mg–Zr Solid Sorbent, Energy Fuels 2013;27(9):5407–5415.
[35]. Ding Y, Song G, Zhu X, Chen R, Liao Q,' Synthesizing MgO with a high specific surface for carbon dioxide adsorption, RSC Adv. 2015;5: 30929-30935.
[36]. Russ JC, Fractal Surfaces (Plenum Press, New York, 1994), pp.178.
[37]. Family F, Vicsek T, Scaling of the active zone in the Eden process on percolation networks and the ballistic deposition model, J. Phys. A: Math. Gen. 1985;18:L75-L81.
[38]. Chauvy PF, Madore C, Landolt D, Variable length scale analysis of surface topography: characterization of titanium surfaces for biomedical applications, Surf. Coat. Technol. 1998;110:48-56.
[39]. Avnir D, Jaroniec M, An isotherm equation for adsorption on fractal surfaces of heterogeneous porous materials, Langmuir 1989;5,6: 1431-1433.
[40]. Dubinin MM, Characterisation of adsorption properties and microporous structures of carbonaceous adsorbents, in Characterization of Porous Solids, Studies in Surface Science and Catalysis, 39, eds. K.K. Unger, J. Rouquerol, K.S.W. Sing and H. Kral (Elsevier, Amsterdam, 1988), pp. 127-139.
[41]. Blancher S, Alie C, Gommes C, Lodewyckx P, Pirard R, Pirard JP, Characterization of silica low density xerogels in presence of additives, in Characterization of Porous Solids VI: Proceedings of the 6th International Symposium on the Characterization of Porous Solids (Allicante, Spain, May 8-11, 2002), pp. 323-331.
[42]. Russ JC, The image processing Cookbook, Second Edition (College of Engineering North Carolina State University, Raleigh, NC, USA, 2011), pp.21.
[43]. Kaneko K, Sato M, Suzuki T, Fujiwara Y, Nishikawa K, Jaroniec M, Surface fractal dimension of microporous carbon fibres by nitrogen adsorption, J. Chem. Soc. Faraday Trans 1991;87:179-184.
[44]. Pfeifer P, Wu YJ, Cole MW, Krim J, Multilayer adsorption on a fractally rough surface, Phys. Rev. Lett. 1989;62:1997-2000.
[45]. Yang D, Krasowska M, Sedev R, Ralston J, The unusual surface chemistry of α-Al_2O_3 (0001), Phys. Chem. Chem. Phys. 2010;12: 13724-13729.
[46]. Wang HY, Ruckenstein E, Carbon dioxide reforming of methane to synthesis gas over supported rhodium catalysts: The effect of support, Appl. Catal. A: Gen. 2000;204:143−152.

Gianina Dobrescu, et. al. "Correlations between the basicity and the fractal dimension of Rh-nanoparticles supported on Al2O3, TiO2 and WO3." *IOSR Journal of Applied Chemistry (IOSR-JAC)*, 14(1), (2021): pp 11-25.